Separable Nonlinear Least Squares Algorithm for Robust Kinematic Calibration of Serial Robots

Chentao Mao[1] · **Zhangwei Chen**[1] · **Shuai Li**[2] · **Xiang Zhang**[3]

Abstract

Kinematic calibration of robots is an effective way to guarantee and promote their performance characteristics. There are many mature researches on kinematic calibration, and methods based on MDH model are the most common ones. However, when employing these calibration methods, it occasionally happens that the objective function cannot converge during iterations. Through analyzing robotic forward kinematics, we found out that the Cartesian coordinates of the end-point are affine to length-related MDH parameters, where linear and nonlinear parameters can be separated. Thanks to the distinctive characteristic of the MDH model, the kinematic calibration problem can be converted into a separable nonlinear least squares problem, which can further be partitioned into two subproblems: a linear least squares problem and a reduced problem involving only nonlinear parameters. Eventually, the optimal structural parameters can be identified by solving this problem iteratively. The results of numerical and experimental validations show that: 1) the robustness during identification procedure is enhanced by eliminating the partial linear structural parameters, the convergence rate is promoted from 68.98% to 100% with different deviation vector pairs; 2) the initial values to be pre-set for kinematic calibration problem are fewer and 3) fewer parameters are to be identified by nonlinear least squares regression, resulting in fewer iterations and faster convergence, where average runtime is reduced from 33.931s to 1.874s.

Keywords Kinematic calibration · Robustness · Separable nonlinear least squares · Positioning accuracy

1 Introduction

As essential ingredients of intelligent manufacturing, industrial robots have been widely employed in a broad array of fine-processing scenarios, such as arc welding [1, 2], robotic grasping [3] and machining [4, 5], which requires ultra-accurate positioning of robots. Unfortunately, since the deviations of rod lengths and zero offsets of each joint are introduced during the manufacturing and assembling procedure, the absolute positioning and orientation errors of robotic end-points are unevenly distributed in the Cartesian space [6, 7]. Hence, it is urgent to identify the structural parameters of robots through kinematic calibration. There are numerous mature methods and algorithms in the field of kinematic calibration [8–10]. However, in practice, it occasionally happened that the objective function of these kinematic calibration methods cannot render to convergence in some situations. The problem we encountered is actually a convergence analysis problem of nonlinear least squares.

It is critical for an optimization problem to choose a suitable model, and it will directly relate to the convergence of the objective function. Considering kinematic calibration of robots, three basic characteristics should be required to meet: completeness, continuity and minimality [11]. So far, there have been several mature modelling theories, and the Denavit-Hartenberg (DH) modelling method [12] is the widely recognized as one of the most well-understood and commonly employed since it has the minimum parameter set representing the location of joint frames. However, it was found out by Hayati [13] that when two consecutive joint axes of robots are nearly parallel or parallel, even a slight change in the geometric structure of robots will

✉ Chentao Mao
mct@zju.edu.cn

[1] State Key Laboratory of Fluid Power and Mechatronic Systems, Zhejiang University, Hangzhou, China

[2] College of Engineering, Swansea University, Swansea, UK

[3] School of Computer Science and Technology, Hangzhou Dianzi University, Hangzhou, China

lead a tremendous deviation in the DH model parameters, and thus it is not continuous. Since then, researchers have modified the modelling approach to overcome the singularity problem, which could be mainly divided into two categories: product of exponential (POE) based model and modified DH (MDH) model. POE based model directly describes the geometry of each joint axis through six parameters, which is singularity-free [14–16]. Nevertheless, there are internal constraints in the six parameters, which will increase the complexity and reduce the robustness of the identification process [17]. Moreover, most robotic controllers have no corresponding compensation interface for POE parameters [18]. Likewise, to solve the singularity problem, some extra redundant parameters were introduced to the DH model, and the Hayati model [19] is the widely used one by adding an angular parameter to rotate around the Y axis of local joint frames, which is also called the MDH model. Since all the correspondences could be found between the robotic geometric structure and MDH model parameters, the identified optimal structural parameters can be readily compensated into robotic controllers. In this paper, all derivations of robotic kinematics will be based on MDH modelling method.

Apparently, the robotic forward kinematics model is a typical nonlinear mapping containing trigonometric functions of structural parameters, and the identification process of structural parameters could be treated as a nonlinear least squares problem. So far, the nonlinear least squares problem has addressed plenty of attentions. With the advantage of fast convergence, one of the most commonly used descent methods in kinematic calibration is the Gauss-Newton method, which can minimize the 2-norm of residual errors based on implemented first derivatives [20]. Then, Levenberg-Marquardt (LM) method [21] was employed to solve the singularity problem that might be encountered during the iterative searching for the optimal parameters with Gauss-Newton method. Recently in [22–24], the absolute positioning accuracy of robots could be further enhanced by the extended Kalman filter method, which can reduce the impact of Gaussian random errors coming with the measurement process. However, when employing these calibration methods, it occasionally happened that the objective function cannot converge during iterations. Through analyzing forward kinematics of robots, we found that the Cartesian coordinates of the end-point are affine to length-related MDH parameters, where linear and nonlinear parameters can be separated. Fortunately, taking advantage of the distinctive structure of the MDH model, the original problem can be turned into a separable nonlinear least squares (SNLLS) problem. Golub and Pereyra [25] firstly proposed the SNLLS problem, and gave its solution through a variable projection method. The key idea of the variable projection method is to partition parameters into linear and nonlinear part [26], among which the linear part of parameters is searched by linear least squares, resulting in a reduced subproblem including only the nonlinear part [27]. Since fewer parameters are to be identified by nonlinear least squares regression, it is crucial to increase the likelihood of finding the global minimum from plenty of other local minimums, and in addition, reduce the time spent searching for the solution [28–30]. In [28], concrete comparisons was presented on the performance of separated algorithms combined with different descent methods, and the influence of different Jacobian matrices on convergence was elaborately given. Based on the benefits described above, we are wondering if the separable nonlinear algorithm can improve the convergence of the robotic kinematic calibration problem, which motivates us to compare the convergence performance of the separable nonlinear algorithm with traditional calibration methods.

The remainder of this paper is organized as follows. In Section 2, the separable nonlinear least squares problem and corresponding solution will be formulated. Section 3 will give the concrete comparisons on numerical and experimental results with different methods on absolute positioning accuracy. Section 4 will conclude this paper. It is worth mentioning that the main contributions lay in:

- Taking advantage of the distinctive characteristic of MDH model, this paper proposes a separable nonlinear least squares algorithm for robotic kinematic calibration. The robustness during identification procedure is enhanced by eliminating the partial linear structural parameters.
- Fewer parameters are to be identified by nonlinear least squares regression, resulting in fewer iterations and faster convergence. In addition, the initial values to be pre-set for kinematic calibration problem are fewer, and thus the convergence of kinematic calibration problem is only related to the pre-set values of robotic nonlinear structural parameters.
- Numerical and Experimental results including comprehensive comparisons substantiate the effectiveness and superiority of the proposed SNLLS algorithm for kinematic calibration.

2 Separable Nonlinear Least Squares Algorithm

In this section, an equivalent MDH model with nonlinear parameters separated will be established, and a separable nonlinear least squares algorithm will be proposed for a faster convergence with wider range.

2.1 Robot-Sensor System for Calibration

The robotic end-effector is expected to attain the desired positioning point. Unfortunately, since the deviations of rod lengths and zero offsets of each joint are introduced during the manufacturing and assembling procedure, the absolute positioning and orientation errors of the tool central point are unevenly distributed in the Cartesian space. Hence, it is critical to promote the performance of robots through identifying the structural parameters.

The experimental apparatus for calibration is presented in Fig. 1, where the Cartesian coordinate of the tool central point (TCP) is accurately measured by a laser tracker. In Fig. 1b, the schematic diagram gives a detailed description of each local frame establishment for a 6-DOF robot, where red arrows represent Z-axes of their local coordinate systems, and blue arrows denote X-axes. For simplicity, the robotic base coordinate system $\{\boldsymbol{M}\}$ is set to coincide with the 1-st joint coordinate system frame when $\theta_1 = 0$. It is worth noting that the transformation of $\{\boldsymbol{B}\}$ with respect to $\{\boldsymbol{M}\}$, namely the hand-eye matrix is unknown, and thus needs to be identified. During the measurement procedure, the TCP successively reaches k arbitrary configurations, whose corresponding Cartesian coordinates should be distributed as much as possible throughout the working space. And then, the coordinates corresponding to each configuration are measured by the laser tracker. In the meantime, joint angles are recorded, which correspond to the k configurations. Finally, with the attained data, the structural parameters can be identified by solving the optimization problem defined in Section 2.3.

2.2 MDH Model with Nonlinear Parameters Separated

According to robotic kinematics, considering a n-DOFs serial robot, the Cartesian coordinate $\boldsymbol{p}_t^{\boldsymbol{m}}$ of the tool central point with respect to the measurement frame $\{\boldsymbol{M}\}$ can be analytically described as follows [31],

$$\boldsymbol{p}_t^{\boldsymbol{m}} = \boldsymbol{f}(\boldsymbol{a}, \boldsymbol{\alpha}, \boldsymbol{\theta}, \boldsymbol{d}, \boldsymbol{\beta}) = \boldsymbol{A}_{\boldsymbol{b}}^{\boldsymbol{m}} \boldsymbol{A}_{\boldsymbol{1}}^{\boldsymbol{b}} \boldsymbol{A}_{\boldsymbol{2}}^{\boldsymbol{1}} \cdots \boldsymbol{A}_{\boldsymbol{n}}^{\boldsymbol{n-1}} \boldsymbol{p}_t^{\boldsymbol{n}}, \tag{1}$$

where $\boldsymbol{f}(\cdot)$ is a nonlinear mapping, providing the connection between MDH parameters $(\boldsymbol{a}, \boldsymbol{\alpha}, \boldsymbol{\theta}, \boldsymbol{d}, \beta)$ and the Cartesian coordinate, $\boldsymbol{p}_t^{\boldsymbol{m}}$. Besides, the homogeneous matrix $\boldsymbol{A}_{\boldsymbol{i}}^{\boldsymbol{i-1}}$ denotes the transformation and rotation from frame $\{\boldsymbol{i-1}\}$ to frame $\{\boldsymbol{i}\}$, and superscript or subscript letters $\boldsymbol{m}$ and $\boldsymbol{b}$ represent the measurement frame $\{\boldsymbol{M}\}$ and robotic base frame $\{\boldsymbol{B}\}$, respectively. The vector $\boldsymbol{p}_t^{\boldsymbol{n}} \in \boldsymbol{R}(3)$ is the Cartesian coordinate of TCP with respect to the n-th joint frame. As mentioned in Section 2.1, the transformation from $\{\boldsymbol{M}\}$ to $\{\boldsymbol{B}\}$, and the Cartesian coordinate of TCP are unknown. Hence, parameters in $\boldsymbol{A}_{\boldsymbol{b}}^{\boldsymbol{m}}$ and $\boldsymbol{p}_t^{\boldsymbol{n}}$ should also be identified and determined. Define that

$$\boldsymbol{A}_{\boldsymbol{b}}^{\boldsymbol{m}} \triangleq \begin{bmatrix} \boldsymbol{R_b} & \boldsymbol{b_b} \\ \boldsymbol{O} & 1 \end{bmatrix}, \tag{2}$$

where

$$\boldsymbol{R_b} = \begin{bmatrix} c\Phi c\Theta & c\phi s\Theta s\Psi - s\Phi c\Psi & c\Phi s\Theta c\Psi + s\Phi s\Psi \\ s\Phi c\Theta & s\Phi s\Theta s\Psi + c\Phi c\Psi & s\Phi s\Theta c\Psi - c\Phi s\Psi \\ -s\Theta & c\Theta s\Psi & c\Theta c\Psi \end{bmatrix}, \tag{3}$$

$$\boldsymbol{b_b} = \begin{bmatrix} X_b & Y_b & Z_b \end{bmatrix}^{\mathrm{T}}, \tag{4}$$

and abbreviations s and c stand for trigonometric functions **sin** and **cos**, respectively. The matrix $\boldsymbol{A}_{\boldsymbol{b}}^{\boldsymbol{m}}$ could be expressed by six parameters to be determined, where $[X_b, Y_b, Z_b]$ and $[\Phi, \Theta, \Psi]$ are respectively transformation and rotation coordinates from $\{\boldsymbol{M}\}$ to $\{\boldsymbol{B}\}$. Besides, $\boldsymbol{p}_t^{\boldsymbol{n}}$ is defined as

$$\boldsymbol{p}_t^{\boldsymbol{n}} \triangleq \begin{bmatrix} X_t & Y_t & Z_t \end{bmatrix}^{\mathrm{T}}, \tag{5}$$

the transformation matrix $\boldsymbol{A}_{\boldsymbol{i}}^{\boldsymbol{i-1}}$ could be expressed according to robotic kinematics, which is elaborated in [31]

$$\boldsymbol{A}_{\boldsymbol{i}}^{\boldsymbol{i-1}} \triangleq \begin{bmatrix} \boldsymbol{R_i} & \boldsymbol{b_i} \\ \boldsymbol{O} & 1 \end{bmatrix}, \tag{6}$$

in which

$$\boldsymbol{R_i} = \begin{bmatrix} c\theta_i c\beta_i - s\theta_i s\alpha_i s\beta_i & -s\theta_i c\alpha_i & c\theta_i s\beta_i + s\theta_i s\alpha_i c\beta_i \\ s\theta_i c\beta_i + c\theta_i s\alpha_i s\beta_i & c\theta_i c\alpha_i & s\theta_i s\beta_i - c\theta_i s\alpha_i c\beta_i \\ -c\alpha_i s\beta_i & s\alpha_i & c\alpha_i c\beta_i \end{bmatrix}, \tag{7}$$

and

$$\boldsymbol{b_i} = \begin{bmatrix} a_i c\theta_i \\ a_i s\theta_i \\ d_i \end{bmatrix} = \begin{bmatrix} c\theta_i & 0 \\ s\theta_i & 0 \\ 0 & 1 \end{bmatrix} \begin{bmatrix} a_i \\ d_i \end{bmatrix}, \tag{8}$$

where a_i, α_i, θ_i, β_i and d_i are MDH parameters corresponding to i-th joint. It is worth noting that the

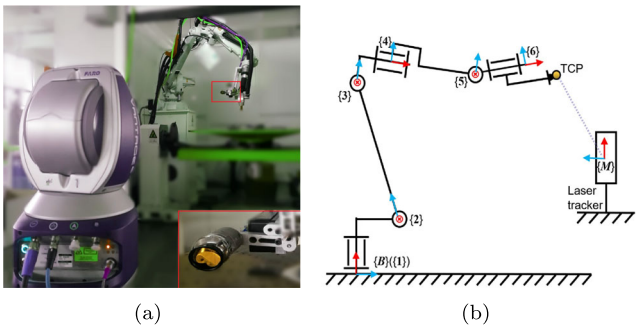

(a) (b)

Fig. 1 Experimental apparatus for kinematic calibration in our lab. **a** Physical map. **b** Schematic diagram

rotation matrix $\boldsymbol{R_i}$ is a function of α_i and θ_i, and the position vector $\boldsymbol{b_i}$ is a function of θ_i, a_i and d_i but is affine to $\left[a_i\ d_i\right]^{\mathrm{T}}$. Thereafter, we have

$$\boldsymbol{x_{i-1}} = \boldsymbol{R_i x_i} + \boldsymbol{b_i}, \tag{9}$$

where $\boldsymbol{x_i}$ denotes the coordinate of TCP in the local coordinate frame of the i-th joint. Then, the coordinate of TCP in the measurement frame can be represented as

$$\begin{aligned}\boldsymbol{x_m} =& \boldsymbol{R_b x_b} + \boldsymbol{b_b} = \boldsymbol{R_b}(\boldsymbol{R_1 x_1} + \boldsymbol{b_1}) + \boldsymbol{b_b} \\ =& \boldsymbol{R_b}\left[\boldsymbol{R_1}(\boldsymbol{R_2 x_2} + \boldsymbol{b_2}) + \boldsymbol{b_1}\right] + \boldsymbol{b_b} \\ =& \boldsymbol{R_b R_1 \cdots R_n x_n} + \boldsymbol{R_b R_1 \cdots R_{n-1} b_n} + \\ & \boldsymbol{R_b R_1 \cdots R_{n-2} b_{n-1}} + \cdots + \boldsymbol{R_b b_1} + \boldsymbol{b_b},\end{aligned} \tag{10}$$

where $\boldsymbol{x_n}$ is equivalent to $\boldsymbol{p_t^n} = [X_t, Y_t, Z_t]^{\mathrm{T}}$, which is the coordinate in the n-th joint frame. For calibration, $\boldsymbol{x_n}$ is constant. $\boldsymbol{x_m}$ is equivalent to $\boldsymbol{p_t^m}$, which is the Cartesian coordinate of TCP in the measurement frame. For calibration, linear and nonlinear parameter vectors to be identified are respectively defined as

$$\boldsymbol{r} = \left[\boldsymbol{b_b}^{\mathrm{T}}, a_1, d_1, \cdots, a_n, d_n, \boldsymbol{x_n}^{\mathrm{T}}\right]^{\mathrm{T}} \in R^{a\times 1}, \tag{11}$$

$$\boldsymbol{\omega} = [\Theta, \Psi, \Phi, \alpha_1, \theta_1, \beta_1 \cdots \alpha_n, \theta_n, \beta_n]^{\mathrm{T}} \in R^{b\times 1}, \tag{12}$$

Define

$$\bar{\boldsymbol{g}}(\boldsymbol{\omega}) \triangleq [\boldsymbol{I}(3), \boldsymbol{g_0}, \boldsymbol{g_1} \cdots, \boldsymbol{g_n}], \tag{13}$$

where

$$\boldsymbol{g_i}(\boldsymbol{\omega}) \triangleq \begin{cases} \boldsymbol{R_b}\begin{bmatrix} c\theta_1 & 0 \\ s\theta_1 & 0 \\ 0 & 1 \end{bmatrix}, & i = 0 \\ [\boldsymbol{R_b R_1 \cdots R_i}]\begin{bmatrix} c\theta_{i+1} & 0 \\ s\theta_{i+1} & 0 \\ 0 & 1 \end{bmatrix}, & 0 < i < n \\ [\boldsymbol{R_b R_1 \cdots R_n}], & i = n \end{cases} \tag{14}$$

Thereafter, the coordinate of TCP in the measurement frame (10) could be rewritten as

$$\begin{aligned}\boldsymbol{x_m} =& \boldsymbol{g_n x_n} + \boldsymbol{g_{n-1}}\begin{bmatrix} a_n \\ d_n \end{bmatrix} + \boldsymbol{g_{n-2}}\begin{bmatrix} a_{n-1} \\ d_{n-1} \end{bmatrix} \\ & + \cdots + \boldsymbol{g_0}\begin{bmatrix} a_1 \\ d_1 \end{bmatrix} + \boldsymbol{b_b},\end{aligned} \tag{15}$$

which can be further simplified into

$$\boldsymbol{x_m} = \bar{\boldsymbol{g}}(\boldsymbol{\omega})\boldsymbol{r}, \tag{16}$$

It is worth noting that $\boldsymbol{x_m}$ is nonlinear in angle-related parameters $\boldsymbol{\omega}$, but affine in length-related parameters $\boldsymbol{r}$.

2.3 Separated Nonlinear Least Squares Problem

For the kinematic calibration problem of serial robots, its objective is to find the optimal structural parameters $\boldsymbol{\omega}$ and $\boldsymbol{r}$ by minimizing the following nonlinear mapping,

$$\begin{aligned}\boldsymbol{c_1}(\boldsymbol{r}, \boldsymbol{\omega}) &= \frac{1}{2}\sum_{j=1}^{k}\left[\boldsymbol{y_m}^{(j)} - \bar{\boldsymbol{g}}(\boldsymbol{\omega})^{(j)}\boldsymbol{r}\right]^2, \\ &= \frac{1}{2}\left\|\boldsymbol{Y_m} - \boldsymbol{G}(\boldsymbol{\omega})\boldsymbol{r}\right\|_2,\end{aligned} \tag{17}$$

where $\boldsymbol{Y_m} = \left[\boldsymbol{y_m}^{\mathrm{T}(1)}, \boldsymbol{y_m}^{\mathrm{T}(2)} \cdots \boldsymbol{y_m}^{\mathrm{T}(k)}\right]^{\mathrm{T}}$, and $\boldsymbol{G}(\boldsymbol{\omega}) = \left[\bar{\boldsymbol{g}}^{\mathrm{T}}(\boldsymbol{\omega})^{(1)}, \bar{\boldsymbol{g}}^{\mathrm{T}}(\boldsymbol{\omega})^{(2)} \cdots \bar{\boldsymbol{g}}^{\mathrm{T}}(\boldsymbol{\omega})^{(k)}\right]^{\mathrm{T}}$. And $\boldsymbol{y_m}^{(j)}$ is the Cartesian coordinate of the TCP with respect to the frame $\{\boldsymbol{M}\}$ measured highly accurately, where $j = 1, 2 \cdots k$ is the sequence number of measurement configurations. In addition, $\boldsymbol{G}(\boldsymbol{\omega})\boldsymbol{r}$ is the corresponding nominal Cartesian coordinate of the TCP, and $\|\cdot\|$ denotes the Euclidean norm. Then, the nonlinear function $\boldsymbol{c_1}$ reflects absolute positioning accuracy of industrial robots. If the nonlinear structural parameter vector $\boldsymbol{\omega}$ is known, the calibration problem turns out a typical linear least squares problem. Therefore, the linear parameter vector $\boldsymbol{r}$ can be directly deduced as

$$\boldsymbol{r} = \boldsymbol{G}(\boldsymbol{\omega})^{+}\boldsymbol{Y_m}, \tag{18}$$

where $\boldsymbol{G}(\boldsymbol{\omega})^{+}$ is a Moore-Penrose inverse of $\boldsymbol{G}(\boldsymbol{\omega})$. Substituting (18) into (17), it can be obtained that

$$\begin{aligned}\boldsymbol{c_2}(\boldsymbol{\omega}) &= \frac{1}{2}\left\|\boldsymbol{Y_m} - \boldsymbol{G}(\boldsymbol{\omega})\boldsymbol{G}(\boldsymbol{\omega})^{+}\boldsymbol{Y_m}\right\|_2 \\ &= \frac{1}{2}\left\|\left(\boldsymbol{I} - \boldsymbol{G}(\boldsymbol{\omega})\boldsymbol{G}(\boldsymbol{\omega})^{+}\right)\boldsymbol{Y_m}\right\|_2 \\ &= \frac{1}{2}\left\|\left(\boldsymbol{I} - \boldsymbol{P}_{\boldsymbol{G}(\boldsymbol{\omega})}\right)\boldsymbol{Y_m}\right\|_2 \\ &= \frac{1}{2}\left\|\boldsymbol{P}^{\perp}_{\boldsymbol{G}(\boldsymbol{\omega})}\boldsymbol{Y_m}\right\|_2 = \frac{1}{2} < \boldsymbol{c}, \boldsymbol{c} >,\end{aligned} \tag{19}$$

where $\boldsymbol{P}_{\boldsymbol{G}(\boldsymbol{\omega})} = \boldsymbol{G}(\boldsymbol{\omega})\boldsymbol{G}(\boldsymbol{\omega})^{+}$, $\boldsymbol{P}^{\perp}_{\boldsymbol{G}(\boldsymbol{\omega})} = \boldsymbol{I} - \boldsymbol{P}_{\boldsymbol{G}(\boldsymbol{\omega})}$ and $\boldsymbol{c} = \boldsymbol{P}^{\perp}_{\boldsymbol{G}(\boldsymbol{\omega})}\boldsymbol{Y_m}$. It is worth noting that the new objective function $\boldsymbol{c_2}(\boldsymbol{\omega})$ is only related to the nonlinear parameter vector $\boldsymbol{\omega}$. In this way, the benefits of separating linear-nonlinear parameters are as follows, 1) the robustness during identification procedure is enhanced by eliminating the partial linear structural parameters; 2) Fewer parameters are to be identified by nonlinear least squares regression, resulting in fewer iterations and faster convergence; and 3) the initial values to be pre-set for calibration problem are fewer. The main process of kinematic calibration is to identify nonlinear parameters $\boldsymbol{\omega}$ first through (19), and then the linear parameters $\boldsymbol{r}$ are calculated by least squares as shown in Eq. 18. Eventually, the objective function of optimization problem for kinematic calibration can be expressed as

$$\underset{\boldsymbol{\omega}}{minimize}: \frac{1}{2}\left\|\boldsymbol{P}^{\perp}_{\boldsymbol{G}(\boldsymbol{\omega})}\boldsymbol{Y_m}\right\|_2, \tag{20}$$

For calibration, taking the 2-norm of absolute positioning errors as the objective function, not only can the errors be

reduced to the greatest extent, but it is minimized that the impact of uncertainty caused by measurement and robotic repeatability errors during the identification procedure.

2.4 Descent Methods and their Jacobian Matrix

Gauss-Newton method is the most common search method used to solve nonlinear least squares problems, and the iterative search process along search direction is

$$^{(\kappa+1)}\boldsymbol{\omega} = {}^{(\kappa)}\boldsymbol{\omega} + {}^{(\kappa)}\boldsymbol{\delta}, \tag{21}$$

where $^{(\kappa)}\boldsymbol{\omega}$ is the current nonlinear structural parameters, and $^{(\kappa+1)}\boldsymbol{\omega}$ is the parameters for next iteration. Superscript κ is the number of loop iterations. The $^{(\kappa)}\boldsymbol{\delta}$ is the search direction, which could be obtained by solving

$$\boldsymbol{J}\left({}^{(\kappa)}\boldsymbol{\omega}\right)^{\mathrm{T}}\boldsymbol{J}\left({}^{(\kappa)}\boldsymbol{\omega}\right)^{(\kappa)}\boldsymbol{\delta} = -\boldsymbol{J}\left({}^{(\kappa)}\boldsymbol{\omega}\right)^{\mathrm{T}}\boldsymbol{c}(\boldsymbol{\omega}), \tag{22}$$

where $\boldsymbol{J}(\boldsymbol{\omega}) \in \boldsymbol{R}^{3k\times a}$ is a Jacobian matrix, describing the differential mapping between structural parameters and Cartesian coordinates of the end-point. Gauss-Newton method is a very efficient method, which can give quadratic convergence in some special cases. However, its convergence is hypersensitive to the initial values of parameters to be identified. Levenberg and later Marquardt proposed a damped least squares method, where both rapidity and robustness are thought and made to the optimal trade-off by introducing a damping parameter μ [32]:

$$\left(\boldsymbol{J}\left({}^{(\kappa)}\boldsymbol{\omega}\right)^{\mathrm{T}}\boldsymbol{J}\left({}^{(\kappa)}\boldsymbol{\omega}\right)+\mu\boldsymbol{I}\right)^{(\kappa)}\boldsymbol{\delta} = -\boldsymbol{J}\left({}^{(\kappa)}\boldsymbol{\omega}\right)^{\mathrm{T}}\boldsymbol{c}, \tag{23}$$

where μ is iteratively updated, whose determination rule can be found in [32]. It can be seen from Eqs. 22 and 23 that the crucial step is to analytically deduce the Jacobian matrix $\boldsymbol{J}(\boldsymbol{\omega})$, which is the first derivative of the error vector $\boldsymbol{c}(\boldsymbol{\omega})$ [28]. It can be calculated by

$$\boldsymbol{J} = D\boldsymbol{P}_{\boldsymbol{G}}^{\perp}\boldsymbol{Y}_{\boldsymbol{m}} = -\boldsymbol{P}_{\boldsymbol{G}}^{\perp}D\boldsymbol{G}\boldsymbol{G}^{-}\boldsymbol{Y}_{\boldsymbol{m}} - \left(\boldsymbol{P}_{\boldsymbol{G}}^{\perp}D\boldsymbol{G}\boldsymbol{G}^{-}\right)^{\mathrm{T}}\boldsymbol{Y}_{\boldsymbol{m}}, \tag{24}$$

where D is the Frechet derivative operator, and $\boldsymbol{G}^{-}$ denotes the symmetric generalized inverse of a matrix $\boldsymbol{G}$.

Proof Since $\boldsymbol{G}$ is a $3k \times a$ matrix function, the following formulas $\boldsymbol{G}\boldsymbol{G}^{-}\boldsymbol{G} = \boldsymbol{G}$ and $(\boldsymbol{G}\boldsymbol{G}^{-})^{\mathrm{T}} = \boldsymbol{G}\boldsymbol{G}^{-}$ will suffice. The Frechet derivative of $\boldsymbol{P}_{\boldsymbol{G}}$ can be given by

$$D\boldsymbol{P}_{\boldsymbol{G}} = D(\boldsymbol{P}_{\boldsymbol{G}}^{2}) = D\boldsymbol{P}_{\boldsymbol{G}}\boldsymbol{P}_{\boldsymbol{G}} + \boldsymbol{P}_{\boldsymbol{G}}D\boldsymbol{P}_{\boldsymbol{G}}, \tag{25}$$

where the two terms on the right can be derived by formulas (28) and (29). Since $\boldsymbol{P}_{\boldsymbol{G}}\boldsymbol{G} = \boldsymbol{G}$, we have

$$D\boldsymbol{G} = D(\boldsymbol{P}_{\boldsymbol{G}}\boldsymbol{G}) = D\boldsymbol{P}_{\boldsymbol{G}}\boldsymbol{G} + \boldsymbol{P}_{\boldsymbol{G}}D\boldsymbol{G}, \tag{26}$$

and hence,

$$D\boldsymbol{P}_{\boldsymbol{G}}\boldsymbol{G} = D\boldsymbol{G} - \boldsymbol{P}_{\boldsymbol{G}}D\boldsymbol{G} = \boldsymbol{P}_{\boldsymbol{G}}^{\perp}D\boldsymbol{G}, \tag{27}$$

Thus, $D\boldsymbol{P}_{\boldsymbol{G}}\boldsymbol{P}_{\boldsymbol{G}}$ can be deduced by

$$D\boldsymbol{P}_{\boldsymbol{G}}\boldsymbol{P}_{\boldsymbol{G}} = D\boldsymbol{P}_{\boldsymbol{G}}\boldsymbol{G}\boldsymbol{G}^{-} = \boldsymbol{P}_{\boldsymbol{G}}^{\perp}D\boldsymbol{G}\boldsymbol{G}^{-}, \tag{28}$$

and

$$\boldsymbol{P}_{\boldsymbol{G}}D\boldsymbol{P}_{\boldsymbol{G}} = (D\boldsymbol{P}_{\boldsymbol{G}}\boldsymbol{P}_{\boldsymbol{G}})^{\mathrm{T}}, \tag{29}$$

Substituting formulas (28) and (29) into (25), it can be obtained that

$$D\boldsymbol{P}_{\boldsymbol{G}} = \boldsymbol{P}_{\boldsymbol{G}}^{\perp}D\boldsymbol{G}\boldsymbol{G}^{-} + \left(\boldsymbol{P}_{\boldsymbol{G}}^{\perp}D\boldsymbol{G}\boldsymbol{G}^{-}\right)^{\mathrm{T}}, \tag{30}$$

Obviously,

$$D\boldsymbol{P}_{\boldsymbol{G}}^{\perp} = -D\boldsymbol{P}_{\boldsymbol{G}}, \tag{31}$$

The proof is thus completed. □

Exploiting corresponding properties of the matrix $\boldsymbol{P}_{\boldsymbol{G}}^{\perp}$, the gradient vector $\boldsymbol{J}^{\mathrm{T}}\boldsymbol{c}$ can be further simplified as

$$\boldsymbol{J}^{\mathrm{T}}\boldsymbol{c} = -\boldsymbol{Y}_{\boldsymbol{m}}{}^{\mathrm{T}}\boldsymbol{P}_{\boldsymbol{G}}^{\perp}D\boldsymbol{G}\boldsymbol{G}^{-}\boldsymbol{Y}_{\boldsymbol{m}}, \tag{32}$$

Proof The right side of Eq. 22 can be expressed as

$$\begin{aligned}\boldsymbol{J}^{\mathrm{T}}\boldsymbol{c} &= -\boldsymbol{Y}_{\boldsymbol{m}}{}^{\mathrm{T}}\left(\boldsymbol{P}_{\boldsymbol{G}}^{\perp}D\boldsymbol{G}\boldsymbol{G}^{-} + \left(\boldsymbol{P}_{\boldsymbol{G}}^{\perp}D\boldsymbol{G}\boldsymbol{G}^{-}\right)^{\mathrm{T}}\right)\boldsymbol{P}_{\boldsymbol{G}}^{\perp}\boldsymbol{Y}_{\boldsymbol{m}}\\ &= term_1 + term_2,\end{aligned} \tag{33}$$

where the two terms on the right will be elaborated in formulas (35) and (37). Since $\boldsymbol{G}^{-}$ is a symmetric generalized inverse of the matrix $\boldsymbol{G}$, it also satisfies $\boldsymbol{G}^{-}\boldsymbol{G}\boldsymbol{G}^{-} = \boldsymbol{G}^{-}$. Then, we have

$$\boldsymbol{G}^{-}\boldsymbol{P}_{\boldsymbol{G}}^{\perp} = \boldsymbol{G}^{-}\left(\boldsymbol{I} - \boldsymbol{G}\boldsymbol{G}^{-}\right) = \boldsymbol{G}^{-} - \boldsymbol{G}^{-}\boldsymbol{G}\boldsymbol{G}^{-} = 0, \tag{34}$$

and hence,

$$term_1 = -\boldsymbol{Y}_{\boldsymbol{m}}{}^{\mathrm{T}}\boldsymbol{P}_{\boldsymbol{G}}^{\perp}D\boldsymbol{G}\boldsymbol{G}^{-}\boldsymbol{P}_{\boldsymbol{G}}^{\perp}\boldsymbol{Y}_{\boldsymbol{m}} = 0, \tag{35}$$

As an idempotent and symmetric matrix $\boldsymbol{P}_{\boldsymbol{G}}^{\perp}$, it meets the following properties

$$\left(\boldsymbol{P}_{\boldsymbol{G}}^{\perp}\right)^{\mathrm{T}}\boldsymbol{P}_{\boldsymbol{G}}^{\perp} = \left(\boldsymbol{P}_{\boldsymbol{G}}^{\perp}\right)^{2} = \boldsymbol{P}_{\boldsymbol{G}}^{\perp} = \left(\boldsymbol{P}_{\boldsymbol{G}}^{\perp}\right)^{\mathrm{T}}, \tag{36}$$

Inserting (36) into the second term, we have

$$\begin{aligned}term_2 &= -\boldsymbol{Y}_{\boldsymbol{m}}{}^{\mathrm{T}}\left(\boldsymbol{P}_{\boldsymbol{G}}^{\perp}D\boldsymbol{G}\boldsymbol{G}^{-}\right)^{\mathrm{T}}\boldsymbol{P}_{\boldsymbol{G}}^{\perp}\boldsymbol{Y}_{\boldsymbol{m}}\\ &= -\boldsymbol{Y}_{\boldsymbol{m}}{}^{\mathrm{T}}\left(D\boldsymbol{G}\boldsymbol{G}^{-}\right)^{\mathrm{T}}\left(\boldsymbol{P}_{\boldsymbol{G}}^{\perp}\right)^{\mathrm{T}}\boldsymbol{P}_{\boldsymbol{G}}^{\perp}\boldsymbol{Y}_{\boldsymbol{m}}\\ &= -\boldsymbol{Y}_{\boldsymbol{m}}{}^{\mathrm{T}}\left(D\boldsymbol{G}\boldsymbol{G}^{-}\right)^{\mathrm{T}}\left(\boldsymbol{P}_{\boldsymbol{G}}^{\perp}\right)^{\mathrm{T}}\boldsymbol{Y}_{\boldsymbol{m}}\\ &= -\boldsymbol{Y}_{\boldsymbol{m}}{}^{\mathrm{T}}\left(\boldsymbol{P}_{\boldsymbol{G}}^{\perp}D\boldsymbol{G}\boldsymbol{G}^{-}\right)^{\mathrm{T}}\boldsymbol{Y}_{\boldsymbol{m}}\\ &= -\boldsymbol{Y}_{\boldsymbol{m}}{}^{\mathrm{T}}\boldsymbol{P}_{\boldsymbol{G}}^{\perp}D\boldsymbol{G}\boldsymbol{G}^{-}\boldsymbol{Y}_{\boldsymbol{m}},\end{aligned} \tag{37}$$

The proof is thus completed. □

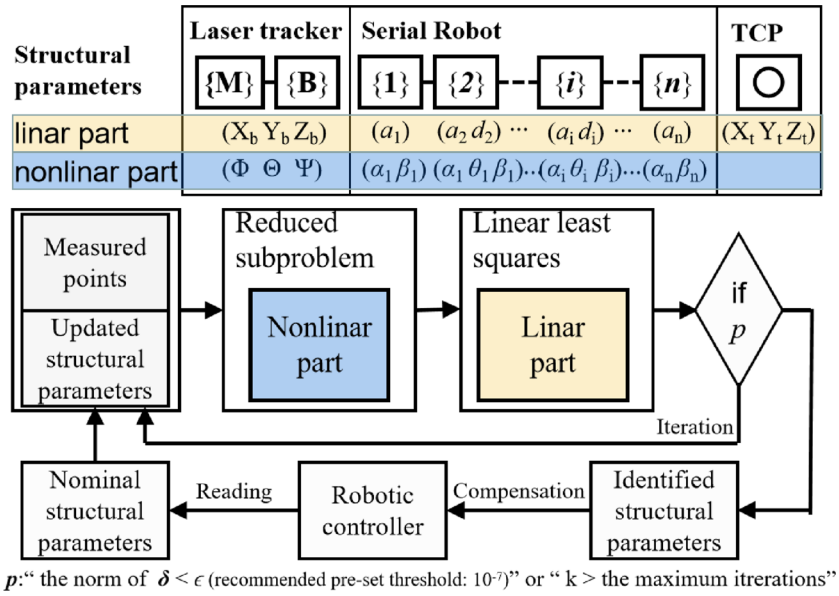

Fig. 2 Schematic diagram of the separable nonlinear least squares algorithm for kinematic calibration

2.5 Separable Nonlinear Least Squares Algorithm

To sum up, the pseudo code of the proposed separable nonlinear least squares algorithm is elaborately presented in Algorithm 1, and corresponding schematic diagram is shown in Fig. 2. On one hand, the search direction of the nonlinear parameter vector $\boldsymbol{\omega}$ is obtained through the separable nonlinear least squares algorithm. On the other hand, substituting the updated nonlinear parameter vector $\boldsymbol{\omega}$ into formula (18), the linear parameter vector $\boldsymbol{r}$ can be directly calculated by linear least squares method. With both linear and nonlinear parameters updated, the objective function (20), namely absolute positioning accuracy can be eventually computed. if the number of iterations is more than M (a pre-set maximum iteration), or the norm of search direction $\|\boldsymbol{\delta}\|_2$ is less than ϵ (a small tolerance), the loop will be terminated, and the iteration number as well as the value of objective function will be saved.

3 Numerical and Experimental Validations

In this section, a set of numerical and experimental validations on 6R serial robots were given to verify the robustness and effectiveness of the proposed algorithm.

3.1 Numerical Validation and Analysis

Note that ABB IRB2600 is generally employed in industrial integrated operations, whose MDH model is presented in Table 1. In the meantime, it can attain command points at any orientation in the work space since it has six independent joints. Hence, we selected ABB IRB2600 as our study subjects. In the simulation, a total of 60 target configurations were randomly generated, considering the measurement noise, structural parameter errors and transmission errors.

Algorithm 1 Separable nonlinear least squares algorithm for robust calibration.

Input: joint angles: $\boldsymbol{\theta}$, nominal nonlinear parameters: ${}^{(0)}\boldsymbol{\omega}$, measured Cartesian coordinates: $\boldsymbol{Y_m}$;
Output: optimal nonlinear parameters: $\boldsymbol{\omega}^*$
initialize ${}^{(0)}\boldsymbol{\omega}$, $\boldsymbol{J}\left({}^{(0)}\boldsymbol{\omega}\right)$, $\boldsymbol{c}\left({}^{(0)}\boldsymbol{\omega}\right)$, ${}^{(0)}\boldsymbol{\delta}$, and ${}^{(0)}\boldsymbol{r}$
while $\boldsymbol{\omega}$ not converge **do**
Separable nonlinear least squares algorithm:
$\boldsymbol{DG}, \boldsymbol{G}, \boldsymbol{G}^{-} \longleftarrow {}^{(\kappa)}\boldsymbol{\omega}, {}^{(\kappa)}\boldsymbol{r}$
$\boldsymbol{J}\left({}^{(\kappa)}\boldsymbol{\omega}\right) = -\boldsymbol{P}_{\boldsymbol{G}}^{\perp}\boldsymbol{DGG}^{-}\boldsymbol{Y_m} - \left(\boldsymbol{P}_{\boldsymbol{G}}^{\perp}\boldsymbol{DGG}^{-}\right)^{\mathrm{T}}\boldsymbol{Y_m}$,
$\boldsymbol{J}\left({}^{(\kappa)}\boldsymbol{\omega}\right)^{\mathrm{T}}\boldsymbol{c}\left({}^{(\kappa)}\boldsymbol{\omega}\right) = -\boldsymbol{Y_m}^{\mathrm{T}}\boldsymbol{P}_{\boldsymbol{G}}^{\perp}\boldsymbol{DGG}^{-}\boldsymbol{Y_m}$,
Obtain search direction $\boldsymbol{\delta}$ by Gauss-Newton method:
${}^{(\kappa)}\boldsymbol{\delta} = -\left(\boldsymbol{J}\left({}^{(\kappa)}\boldsymbol{\omega}\right)^{\mathrm{T}}\boldsymbol{J}\left({}^{(\kappa)}\boldsymbol{\omega}\right)\right)^{+}\boldsymbol{J}\left({}^{(\kappa)}\boldsymbol{\omega}\right)^{\mathrm{T}}\boldsymbol{c}(\boldsymbol{\omega})$,
or Levenberg-Marguardt method:
${}^{(\kappa)}\boldsymbol{\delta} = -\left(\boldsymbol{J}\left({}^{(\kappa)}\boldsymbol{\omega}\right)^{\mathrm{T}}\boldsymbol{J}\left({}^{(\kappa)}\boldsymbol{\omega}\right) + \mu\boldsymbol{I}\right)^{+}\boldsymbol{J}\left({}^{(\kappa)}\boldsymbol{\omega}\right)^{\mathrm{T}}\boldsymbol{c}(\boldsymbol{\omega})$,
${}^{(\kappa+1)}\boldsymbol{\omega} = {}^{(\kappa)}\boldsymbol{\omega} + {}^{(\kappa)}\boldsymbol{\delta}$,
Updating of states $\boldsymbol{\omega}$, and calculation of linear parameters $\boldsymbol{r}$ by least squares:
${}^{(\kappa+1)}\boldsymbol{r} = \boldsymbol{G}({}^{(\kappa+1)}\boldsymbol{\omega})^{+}\boldsymbol{Y_m}$,
Updating of states $\boldsymbol{r}$, and objective function:
$\boldsymbol{c_2}(\boldsymbol{\omega}) = \frac{1}{2}\left\|\boldsymbol{P}_{\boldsymbol{G}(\boldsymbol{\omega})}^{\perp}\boldsymbol{Y_m}\right\|_2$,
end while

The performance of the proposed algorithm in Section 2 was compared to the nonlinear least squares algorithm presented in Algorithm 2. It can be seen in Algorithm

Algorithm 2 Nonlinear least squares algorithm.

Input: joint angles: $\boldsymbol{\theta}$, nominal parameters: ${}^{(0)}\boldsymbol{l} = [{}^{(0)}\boldsymbol{\omega}, {}^{(0)}\boldsymbol{r}]$, measured Cartesian coordinates: $\boldsymbol{Y_m}$;
Output: optimal structural parameters: $\boldsymbol{l}^*$
initialize ${}^{(0)}\boldsymbol{l}$ *and* $\widetilde{\boldsymbol{J}}\left(\boldsymbol{\theta}, {}^{(0)}\boldsymbol{l}\right)$
while $\boldsymbol{l}$ not converge **do**
Nonlinear least squares algorithm:
$${}^{(\kappa)}\boldsymbol{x_m} = \widetilde{\boldsymbol{G}}\left(\boldsymbol{\theta}, {}^{(\kappa)}\boldsymbol{l}\right),$$
$$\widetilde{\boldsymbol{c}}({}^{(\kappa)}\boldsymbol{l}) = \boldsymbol{Y_m} - \widetilde{\boldsymbol{G}}\left(\boldsymbol{\theta}, {}^{(\kappa)}\boldsymbol{l}\right),$$
$$\widetilde{\boldsymbol{J}}\left(\boldsymbol{\theta}, {}^{(\kappa)}\boldsymbol{l}\right) = \partial\widetilde{\boldsymbol{c}}({}^{(\kappa)}\boldsymbol{l})/\partial\boldsymbol{l}^{\mathrm{T}} = -\partial\widetilde{\boldsymbol{G}}(\boldsymbol{\theta}, {}^{(\kappa)}\boldsymbol{l})/\partial\boldsymbol{l}^{\mathrm{T}},$$
Obtain search direction $\boldsymbol{\delta}$ by Gauss-Newton method:
$${}^{(\kappa)}\widetilde{\boldsymbol{\delta}} = -\left(\widetilde{\boldsymbol{J}}\left({}^{(\kappa)}\boldsymbol{l}\right)^{\mathrm{T}}\widetilde{\boldsymbol{J}}\left({}^{(\kappa)}\boldsymbol{l}\right)\right)^{+}\widetilde{\boldsymbol{J}}\left({}^{(\kappa)}\boldsymbol{l}\right)^{\mathrm{T}}\widetilde{\boldsymbol{c}}(\boldsymbol{l}),$$
or Levenberg-Marguardt method:
$${}^{(\kappa)}\widetilde{\boldsymbol{\delta}} = -\left(\widetilde{\boldsymbol{J}}\left({}^{(\kappa)}\boldsymbol{l}\right)^{\mathrm{T}}\widetilde{\boldsymbol{J}}\left({}^{(\kappa)}\boldsymbol{l}\right) + \mu\boldsymbol{I}\right)^{+}\widetilde{\boldsymbol{J}}\left({}^{(\kappa)}\boldsymbol{l}\right)^{\mathrm{T}}\widetilde{\boldsymbol{c}}(\boldsymbol{l}),$$
$${}^{(\kappa+1)}\boldsymbol{l} = {}^{(\kappa)}\boldsymbol{l} + {}^{(\kappa)}\widetilde{\boldsymbol{\delta}},$$
Updating of states $\boldsymbol{l}$, and objective function:
$$\widetilde{\boldsymbol{c_2}}(\boldsymbol{\omega}) = \frac{1}{2}\left\|\boldsymbol{Y_m} - \widetilde{\boldsymbol{G}}\left(\boldsymbol{\theta}, \boldsymbol{l}\right)\right\|_2,$$
end while

II that both linear and nonlinear parameters are treated as nonlinear, and the first derivative of robotic forward kinematics is deduced and treated as the Jacobian matrix. Eventually, the optimal structural parameters are obtained by iteratively searching the descent direction. According to different descent methods, Algorithm 2 can be divided into nonlinear Gauss-Newton method and nonlinear Levenberg-Marguardt method, abbreviated as NLGS and NLLM, respectively. Likewise, separable nonlinear Gauss-Newton method and separable nonlinear Levenberg-Marguardt method are abbreviated as SNLGS and SNLLM, respectively. During the robotic calibration procedure of the actual application scenario, it is almost impossible to know the exact transformation from $\{\boldsymbol{M}\}$ to $\{\boldsymbol{B}\}$, and the Cartesian coordinates of TCP with respect to frame $\{\boldsymbol{n}\}$. Hence, the initial values of $\boldsymbol{A}_b^m$ and $\boldsymbol{p}_t^n$ were set as $\boldsymbol{I}(4)$ and $[0, 0, 0, 1]^{\mathrm{T}}$, respectively. And initial MDH parameters were set to nominal values. Besides, the maximum iteration M was set to 10000.

Table 1 MDH Parameters of an ABB 2600 robot

Joint	a	d	θ	α	β
1	150	445	0	$-\pi/2$	0
2	900	0	$-\pi/2$	0	0
3	150	0	0	$-\pi/2$	0
4	0	938	0	$\pi/2$	0
5	0	0	π	$\pi/2$	0
6	0	200	0	0	0

Table 2 Comparisons on convergence with various methods

Indicator	NLGN	NLLM	SNLGN	SNLLM
Avg iteration num	144.15	4595.27	13.94	26.90
Avg RMS/mm	77.579	1.493	1.493	1.493
Avg runtime/s	5.933	33.931	0.927	1.874
Convergence rate/%	92.89	68.98	100	100
Rate of convergence to minimum/%	74.35	68.98	100	100

To verify the efficiency and robustness of the proposed algorithm, numerical validation was conducted with different pre-set MDH parameters, θ_2 and α_3. A deviation vector pair $[\Delta\theta_2, \Delta\alpha_3]$ was added to the nominal MDH parameters, where both $\Delta\theta_2$ and $\Delta\alpha_3$ are chosen from $-3.1rad$ to $3.1rad$ with an interval of $0.1rad$. Table 2 gives comprehensive comparisons on convergence with different methods. For NLGN and NLLM method, there existing situations that the initial MDH parameters with some deviation vector pairs added that cannot achieve a convergence, even when the number of iterations reaches the maximum, reflecting in convergence rates of them are 92.89% and 68.98%, respectively. Besides, other deviation vector pairs with NLGN method converge to the local minimum, instead of the global minimum, resulting in the rate of convergence to minimum of NLGN method is only 74.35%. By the way, the calculation processes of average iteration number and average root mean squares (RMS) error exclude the deviation vector pairs not convergent. It can be concluded that for the separable nonlinear least squares algorithm, whether it is Gauss-Newton method or LM method can achieve a fast global convergence. Apparently, SNLGN method with fewer iterations spends less time to obtain the goal than SNLLM method.

Concrete iteration number and convergence situations are presented in Fig. 3. In 3D colormap surfaces, there are various deviation vector pairs $[\Delta\theta_2, \Delta\alpha_3]$ in the 'X-Y plane', and the number of iterations on the 'Z axis'. It can be seen that when the norm of the deviation vector pairs is small, faster convergence can be achieved, reflecting in the blue regions in Fig. 3a, b and d. Since the objective functions corresponding to Algorithms 1 and 2 are different, it is necessary to determine a physically meaningful and universal indicator to equivalently replace the objective functions. Here in heatmaps, the absolute positioning root mean squares error of robots is chosen to represent the convergence value corresponding to the objective function, which reflects in the color scale. In addition, the deviation vector pairs not convergent reflect in heatmaps in the form of white dots. A very interesting phenomenon can be found in Fig. 3 that although the convergence rate of NLLM method is lower than that of NLGN method, all convergent deviation

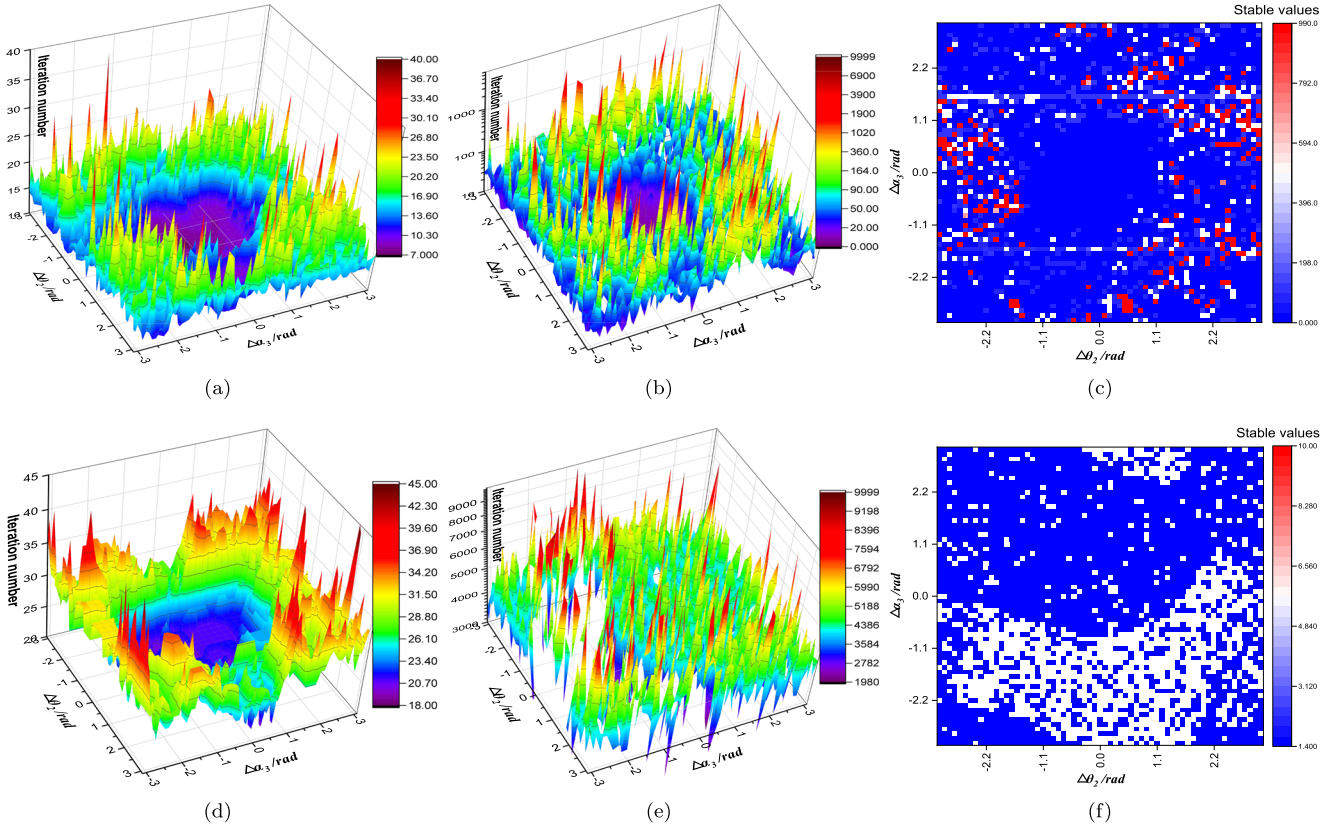

Fig. 3 Comparisons on convergence domain among NLGN, NLLM, SNLGN and SNLLM methods. **a** 3D colormap surface of iteration number required for the objective function to converge with different pre-set deviation vector pairs with SNLGN method. **b** 3D colormap surface of iteration number with NLGN method. **c** Heatmap of the convergence values with different pre-set deviation vector pairs with NLGN method. **d** 3D colormap surface of iteration number with SNLLM method. **e** 3D colormap surface of iteration number with NLLM method. **f** Heatmap of convergence values with NLLM method

vector pairs of NLLM method can achieve convergence to minimum. We can reasonably guess that the non-convergent deviation vector pairs in Fig. 3f, if there is a large enough number of iterations, can eventually achieve convergence to the minimum. Some of these deviation vector pairs are verified in Fig. 4. We can conclude that if the linear and nonlinear parameters are not separated, the rate of convergence to minimum of NLLM method may be higher than that of NLGN method, but it will take much more time to realize the convergence.

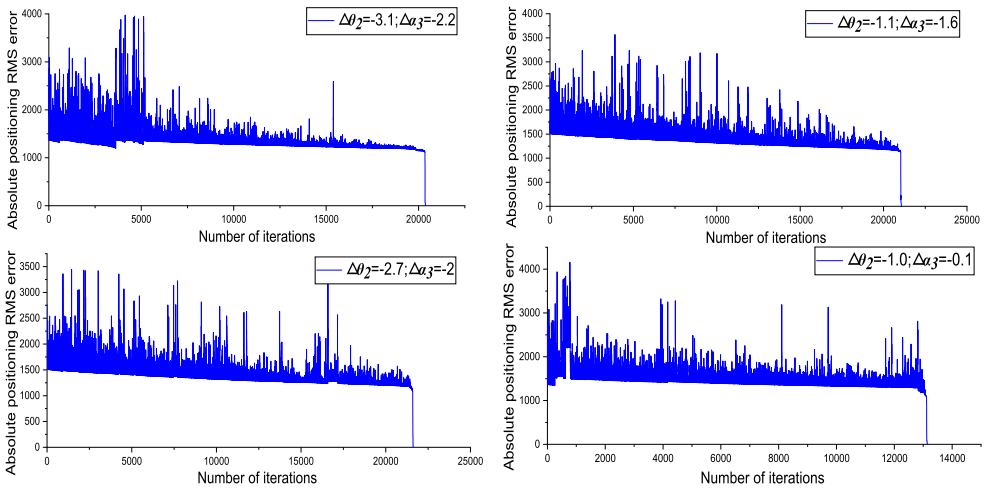

Fig. 4 Calibration processes of NLLM method on non-convergent deviation vector pairs within 10000 iterations

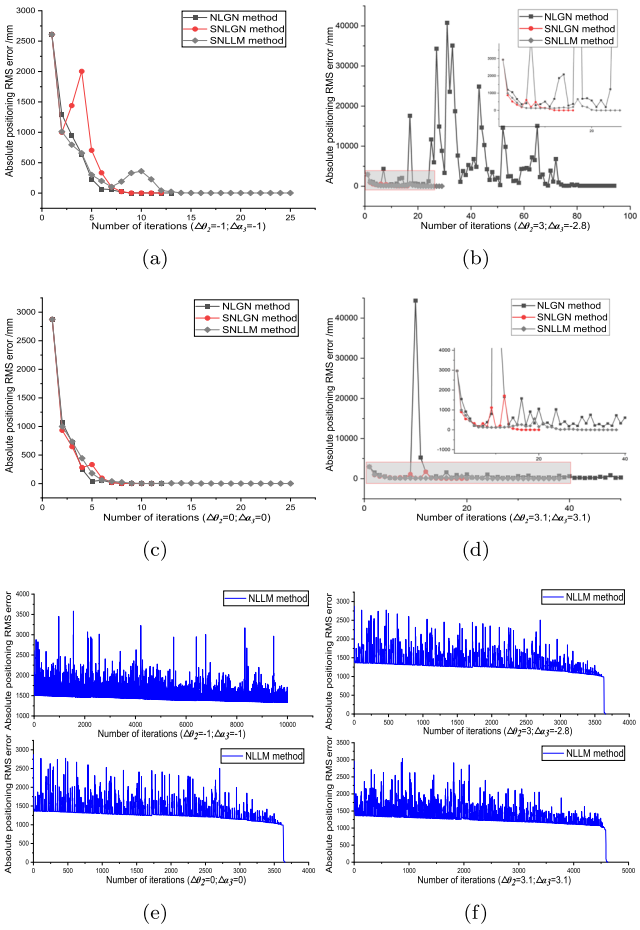

Fig. 5 Comparisons on calibration processes among the four methods. **a** Comparisons among NLGN, SNLGN and SNLLM methods with the initial pre-set deviation vector pair $[-1, -1]$. **b** Deviation vector pair $[3, -2.8]$. **c** Deviation vector pair $[0, 0]$. **d** Deviation vector pair $[3.1, 3.1]$. (e) Calibration processes of NLLM method with deviation vector pairs $[-1, -1]$ and $[0, 0]$. **f** NLLM method with deviation vector pairs $[3, -2.8]$ and $[3.1, 3.1]$

In Fig. 5, to reflect the distinction in the calibration procedure of parameter identification, iteratively calibration results with different methods are presented. A total of four certain deviation vector pairs were chosen, which can comprehensively reflect all situations encountered by different optimization methods. It can be seen in Fig. 5a that all the three methods could render to convergence quickly with the initial pre-set deviation vector pair of $[-1, -1]$. However, the objective function of NLLM method is still far away from the global minimum even with the iteration number of 10000. In Fig. 5b and f, only NLLM, SNLGN and SNLLM methods are globally convergent, and the absolute positioning root mean squares error of NLGN method is convergent to $107.99mm$, obviously not the global minimum. As for the deviation vector pair of $[0, 0]$, all the four methods can realize global convergence. For the deviation vector pair of $[3.1, 3.1]$, except NLGN method has not yet converged reaching the maximum iteration number, all other methods can achieve convergence to minimum. In addition, employing the methods with nonlinear structural parameters separated, the indicator function will not violently oscillate during the process of iteratively searching for the optimal structural parameters, which could increase the robustness of parameter identification procedure.

To sum up, both SNLGN and SNLLM methods can achieve global convergence in the numerical validation. Considering the runtime and convergence, SNLGN method has the best performance among the four methods. The main advantages of kinematic calibration based on MDH model with nonlinear parameters separated lay in that: 1) The robustness during identification procedure of nonlinear parameters is enhanced by eliminating the partial linear structural parameters; 2) Linear structural parameters can readily be obtained by mature linear least squares; 3) Fewer parameters are to be identified by nonlinear least squares regression, resulting in fewer iterations and faster convergence; and 4) the required initial values to be pre-set for calibration problem are fewer, and the convergence of kinematic calibration is only related to the pre-set values of nonlinear parameters.

3.2 Experimental Validation with Various Methods

The kinematic calibration experiment was conducted on an ABB IRB2600 robot as shown in Fig. 1a. Considering that there might be some other unknown sources of nonlinear noise during the measurement of robots, a set of 100 configurations were selected and measured as experimental data for kinematic calibration. Comparisons on calibration processes among the four methods mentioned in Section 3.2 are depicted in Fig. 6. Except the NLLM method, all the other methods can achieve convergence to the minimum in searching the optimal structural parameters. Likewise, SNLGN method has the best performance with the fastest convergence. Moreover, the methods with nonlinear parameters unseparated have obvious oscillation phenomenon during the iterations.

The optimal structural parameters were obtained through SNLGN method, and the experimental calibration result of absolute positioning accuracy is presented in Fig. 7. It can be seen that the absolute positioning accuracy is dramatically improved by 72.46%, which meets the requirement of most industrial production and manufacturing tasks.

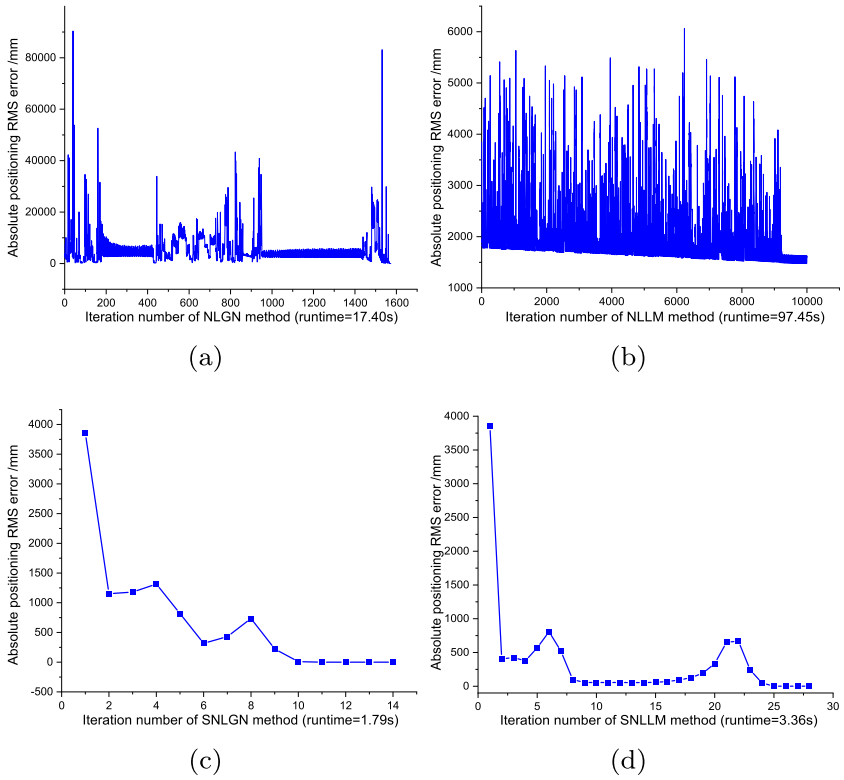

Fig. 6 Comparisons on calibration processes among NLGN, NLLM, SNLGN and SNLLM methods with the same experimental data. **a** Calibration process of NLGN method. **b** NLLM method. **c** SNLGN method. **d** SNLLM method

4 Conclusion

In this paper, a robust kinematic calibration algorithm with nonlinear parameters separated is proposed. The novel feature is that, by separating the linear and nonlinear structural parameters of robots, the original problem of kinematic calibration can be partitioned into two subproblems: a linear least squares subproblem and a reduced subproblem involving only nonlinear parameters. For the former one, linear structural parameters can readily be obtained by mature linear least squares; For the latter one, the robustness during identification procedure of nonlinear parameters is enhanced by eliminating the partial linear structural parameters, and fewer parameters are to be identified by nonlinear least squares regression, resulting in fewer iterations and faster convergence. The results of numerical and experimental validations show that: 1) the convergence rate is promoted from 68.98% to 100% with different deviation vector pairs; and 2) the average running time is reduced from 33.931s to 1.874s.

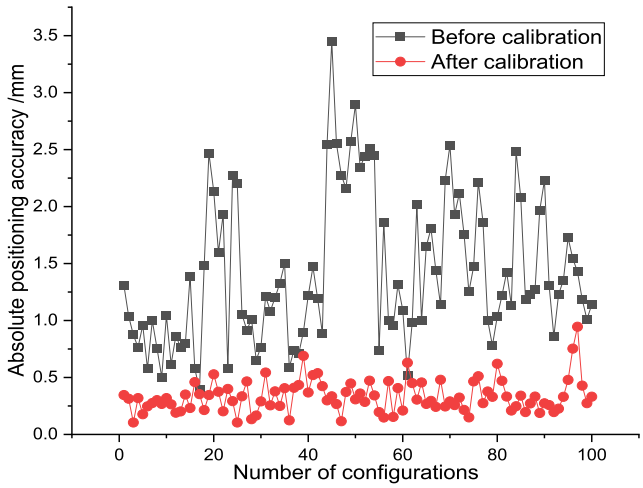

Fig. 7 Experimental calibration result of absolute positioning accuracy with the optimal structural parameters

Acknowledgements This work was supported by the 2017 National Key R&D Program of China (No.2017YFB1301400).

Compliance with Ethical Standards

Conflict of interests The authors declare that they have no conflict of interest.

References

1. Le, J., Zhang, H., Chen, X., Xiong, G.: Rectangular fillet weld tracking by robots based on rotating arc sensors in gas metal arc welding. Int. J. Adv. Manuf. Technol. **93**(4), 1–14 (2017)
2. Yu, Z., He, Y., Xu, Y., Chen, H.: Vision-based deviation extraction for three-dimensional control in robotic welding with steel sheet. Int. J. Adv. Manuf. Technol. **95**(9–12), 4449–4458 (2018)

3. Levine, S., Pastor, P., Krizhevsky, A., Quillen, D.: Learning hand-eye coordination for robotic grasping with deep learning and large-scale data collection. In: International Symposium on Experimental Robotics (2016)
4. Kim, S., Nam, E., Ha, T., et al.: Robotic machining: A review of recent progress. Int. J. Precis. Eng. Manuf. **20**(9), 1629–1642 (2019)
5. Lin, Y., Zhao, H., Ding, H.: Posture optimization methodology of 6R industrial robots for machining using performance evaluation indexes. Robot. Comput. Integr. Manuf. **48**, 59–72 (2017)
6. Mao, C., Li, S., Chen, Z., et al.: A novel algorithm for robust calibration of kinematic manipulators and its experimental validation. IEEE Access **7,** 90487–90496 (2019)
7. Mao, C., Li, S., Chen, Z., et al.: Robust kinematic calibration for improving collaboration accuracy of dual-arm manipulators with experimental validation. IEEE Access, 155 (2020)
8. Li, C., Wu, Y., Lowe, H., Li, Z.: POE-based robot kinematic calibration using axis configuration space and the adjoint error model. IEEE Trans. Robot. **32**(5), 1264–1279 (2016)
9. Jiang, Z., Zhou, W., Li, H., et al.: A new kind of accurate calibration method for robotic kinematic parameters based on extended Kalman and particle filter algorithm. IEEE Trans. Indus. Electron. **65**(4), 3337–3345 (2018)
10. Brau-Avila, A., Acero, R., Santolaria, J., Valenzuela-Galvan, M., et al.: Kinematic parameter identification procedure of an articulated arm coordinate measuring machine based on a metrology platform. Int. J. Adv. Manuf. Technol. **104**(1), 1027–1040 (2019)
11. Schröer, K., Albright, S., Grethlein, M.: Complete, minimal and model-continuous kinematic models for robot calibration. Robot. Comput.-Integr. Manuf. **13**(1), 73–85 (1997)
12. Denavit, J., Hartenberg, R.: A kinematic notation for lower-pair mechanisms based on matrices. J. Appl. Mech. **22**, 215–221 (1955)
13. Hayati, S., Mirmirani, M.: Improving the absolute positioning accuracy of robot manipulators. J. Field Robot. **2**(4), 397–413 (1985)
14. Wu, L., Yang, X., Chen, K., Ren, H.: A minimal POE-based model for robotic kinematic calibration with only position measurements. IEEE Trans. Autom. Sci. Eng. **12**(2), 758–763 (2015)
15. Tao, P., Yang, G.: Calibration of industrial robots with product-of-exponential (POE) model and adaptive Neural Networks. IEEE International Conference on Robotics and Automation (2015)
16. He, R., Li, X., Shi, T., et al.: A kinematic calibration method based on the product of exponentials formula for serial robot using position measurements. Robotica **33**(6), 1–19 (2015)
17. Chen, G., Wang, H., Lin, Z.: Determination of the identifiable parameters in robot calibration based on the POE formula. IEEE Trans. Robot. **5**, 30 (2014)
18. Li, C., Wu, Y., Li, Z.: Identifiability and improvement of adjoint error approach for serial robot calibration. In: IEEE International Conference on Robotics and Automation (2014)
19. Samad, A., Hayati, S.: Robot arm geometric link parameter estimation. IEEE Conference on Decision and Control (1983)
20. Wang, X., Li, D., Wang, M.: Complete calibration of industrial robot with limited parameters and neural network. IEEE International Symposium on Robotics and Intelligent Sensors (2016)
21. Motta, J., Carvalho, G., Mcmaster, R.: Robot calibration using a 3D vision-based measurement system with a single camera. Robot. Comput. Integr. Manuf. **17**(6), 487–497 (2001)
22. Du, G., Ping, Z.: Online serial manipulator calibration based on multisensory process via extended Kalman and particle filters. Trans. Indus. Electron. **61**(12), 6852–6859 (2014)
23. Du, G., Zhang, P., Li, D.: Online robot calibration based on hybrid sensors using Kalman Filters. Roboti. Comput. Integr. Manuf. **31**, 91–100 (2015)
24. Jiang, Z., Zhou, W., Li, H., Mo, Y., Ni, W., Huang, Q.: A new kind of accurate calibration method for robotic kinematic parameters based on the extended Kalman and particle filter. Trans. Indus. Electron. **65**(4), 3337–3345 (2018)
25. Golub, G., Pereyra, V.: The differentiation of pseudo-inverses and nonlinear least squares problems whose variables separate. SIAM J. Numer. Anal. **10**(2), 413–432 (1973)
26. O'Leary, D., Rust, B.: Variable projection for nonlinear least squares problems. Comput. Optim. Appl. **54**(3), 579–593 (2013)
27. Golub, G., Pereyra, V.: Separable nonlinear least squares: the variable projection method and its applications. Inverse Probl. **19**, 2 (2003)
28. Gan, M., Chen, C., Chen, G., Chen, L.: On some separated algorithms for separable nonlinear least squares problems. IEEE Trans. Cybern. **48**(10), 2866–2874 (2018)
29. Chung, J., Nagy, J.: An efficient iterative approach for large-scale separable nonlinear inverse problems. SIAM J. Sci. Comput. **31**(6), 4654–4674 (2010)
30. Min, G., Li, H.: An efficient variable projection formulation for separable nonlinear least squares problems. IEEE Trans. Cybern. **44**(5), 707–711 (2014)
31. Siciliano, B.: Robotics: Modelling, Planning and Control. Springer, London (2009)
32. Ruszczynski, A.: Nonlinear Optimization. Princeton University Press (2006)

Chentao Mao received the B.E. degree in Mechatronic Engineering from University of Electronic Science and Technology of China, Chengdu, China, in 2015. He is currently working towards the Ph.D degree in Mechanical electronics at department of Mechanical Engineering, Zhejiang University, Hangzhou, China. His current research interests include kinematic calibration, optimization theory and control.

Zhangwei Chen received the B.S. degree in Scientific Instruments and the Ph.D. degree in mechanical engineering from Zhejiang University, Hangzhou, China, in 1986 and 1995. And currently, he is a professor at the faculty of mechanical engineering and automation at Zhejiang University. His research interests include vibration and control, signal sensing and analysis, and measurement and calibration for robots.

Shuai Li received the B.E. degree in precision mechanical engineering from the Hefei University of Technology, Hefei, China, the M.E. degree in automatic control engineering from the University of Science and Technology of China, Hefei, China, and the Ph.D. degree in electrical and computer engineering from the Stevens Institute of Technology, Hoboken, NJ, USA. He is currently an Associate Professor in robotics and autonomous systems with the College of Engineering, Swansea University, UK. His current research interests include robot arm manipulation and calibration, impedance/admittance control, human-robot interaction, dynamic neural networks. Dr. Li served as the General Co-Chair of 2018 International Conference on Advanced Robotics and Intelligence Control, and is now serving as the Editor-in-Chief of International Journal of Robotics and Control.

Xiang Zhang received the Ph.D degree in Mechatronics Engineering from Zhejiang University, Hangzhou, China, in 2014. He is currently a teacher in school of computer science and technology, Hanzhou Dianzi University, Hangzhou, China. His current research interests include kinematic calibration, computer vision and real-time system.